Phase-Coupling Effects in Three-Phase Inductive Fault-Current Limiter Based on Permanent Magnets

J. Linden, Y. Nikulshin, A. Friedman, Y. Yeshurun, and S. Wolfus

Laboratory for Magnetic Measurements, Department of Physics, Institute of Superconductivity, Bar-Ilan University, Ramat-Gan 5290002, Israel

In this article, a novel concept of an inductive, saturated-core fault-current limiter (FCL) design is presented, capable of limiting three-phase faults. The design is based on high-remanence permanent magnets for biasing high-saturation electrical steel cores, thus minimizing the device volume, dimensions, and cost and allowing a relatively easy assembly process due to the magnetic symmetry of the model. By implementing a three-phase design in a single device, we harness the full potential of each magnet, substantially reducing the required material for achieving negligible losses during nominal operation while increasing current limiting during faults. A laboratory-scale, low-voltage prototype has been built and tested to prove the feasibility of the new concept, suggesting that upscaling to higher voltage devices is plausible. Extensive simulations, using finite-element analysis, have yielded insight into several measured phenomena, including a unique phase-coupling effect experienced during three-phase fault measurements.

Index Terms—**Fault current limiters (FCLs), magnetic saturation, permanent magnets, triple phase.**

I. Introduction

DEVELOPMENT and characterization of fault-current limiters (FCLs) have been fast paced in recent years. This is mainly due to the increase in demand for a capable and efficient system that can deal with the ever-increasing electrical network demands. The industry is moving into an era that is not only continuously increasing its energy demands but is also aimed at integrating a variety of smart grids [1]. On combining high-power grids and multidirectional energy flow (where the networks include consumer production and renewable energy generation sources), the prospect of fault states increases drastically. If available, higher power circuit breakers are a costly solution that requires major bus and device upgrades. While they provide a disconnecting solution, they also allow for higher fault currents in the distribution equipment, which would be subjected to much higher stresses than originally designed for those in [2], thus even increasing the volatility of a fault event. The FCL provides an optimal solution for these challenges, providing low power loss for normal grid performance when obtaining high current limiting capabilities in the case of a fault grid state. One of the prevailing FCL concepts is the saturated-core inductive FCL (SCFCL) [3]–[6]. The method of operation for the SCFCL function is by altering the impedance of coils in series with the electrical grid by means of introducing variable saturation levels of the magnetic cores. This changes the permeability within the core from a saturated (low permeability) to a nonsaturated (high permeability) state, affecting, in turn, the inductance of the ac coils. This concept has proven very effective in fault-current limiting [7] and has already been implemented in FCL devices installed in live grids [8], [9].

SCFCLs present a unique operational capability that promotes them as a viable solution for limiting fault currents. Under normal grid conditions, the SCFCL retains low impedance so that the power flow is not disturbed, and operational losses are negligible. In an event of a fault, however, the SCFCL impedance rapidly and passively increases, becoming an instantaneous high impedance reactor, thus limiting the overall prospected fault current. This can allow a lower scaled circuit breaker to be jointly used with the SCFCL device, or alternatively saves the need for upgrading breakers in a line where prospective fault currents approach or have already exceeded existing infrastructure breaker ratings.

The SCFCL is a technology that presents several advantages desired in a device or system which can limit the fault current in the power system [10]: it limits the first peak of the fault current, exhibits low impedance and low energy operational losses in the normal state, generates no unacceptable harmonics in the normal state, exhibits a smooth and gradual change of impedance from the normal mode to the fault mode and vice versa, and it has a short ("zero") recovery time. Furthermore, the lack of superconducting to normal phase transition or active electronic components makes it practically a fail-safe device where under no scenario can an unlimited fault current pass through the device without being clipped by the device's fault impedance.

Although the common SCFCL upholds the full functionality requirements mentioned above, it suffers from several disadvantages. The most significant is the high level of runtime maintenance, and the nominal runtime energy losses are the result of the powerful dc coils that common SCFCLs are usually equipped with as a means of controlling the magnetic field within the magnetic cores. This introduces resistive losses for regular wiring, or in the case of superconductive coils, energy losses due to the need for cooling the superconductors to cryogenic temperatures, as well as for maintenance.

Manuscript received April 30, 2019; revised September 9, 2019 and November 9, 2019; accepted November 21, 2019. Date of current version January 20, 2020. Corresponding author: J. Linden (e-mail: lindenjhn@gmail.com).

This article has supplementary downloadable material available at http://ieeexplore.ieee.org, provided by the authors.

Color versions of one or more of the figures in this article are available online at http://ieeexplore.ieee.org.

Digital Object Identifier 10.1109/TMAG.2019.2956147

It is primarily for these reasons that implementing permanent magnets, as a means for controlling the core's magnetic saturation levels, becomes attractive.

Several permanent-magnet SCFCL designs have been developed and tested [10]–[16]; however, they have not yet achieved the level of mass implementation in electrical grids. This may be due to the complicated processes involved in the design and construction of the devices, especially when upscaling the design to be used for high power grid points [17]. When comparing the volume of materials and complexity of assembling the device with the current-limiting capabilities, alternate FCL technologies have proven more desirable. The reasons for this complexity lie in the use of permanent magnets themselves. Once a high remanence permanent magnet move toward the nonsaturated ferromagnetic material (such as the iron core), the attracting forces proportional to $(\vec{B} \cdot \frac{d\vec{B}}{dx})$ increase enormously. This results in the complexity of aligning the permanent magnets with the proper orientation during the assembly process. As the device would be meant for increasingly larger voltages as the electrical grid progresses, the dimensions of the permanent magnets dealing with would make the assembly nearly impossible and extremely hazardous. A suitable solution for this is to use permanent magnets with less remanence such as ceramic ferrites. This provides slightly different magnetic dynamics as considered in [12]. The inherit consequence for using lower remanence materials is that it directly leads to a massive increase in the total dimensions and materials needed, further complicating the assembly process.

In this article, we propose a design that uses high remanence permanent magnets, as well as high saturation electrical steel cores, presented in a novel configuration of the cores and magnets that result in a very efficient system capable of limiting single- to three-phase faults. Extensive magnetic simulations were used to determine optimal geometry and materials, and a small laboratory-scale prototype has been built and tested, resulting in promising results from all aspects most importantly relative compactness, high capabilities, and ease of assembly. Sections III and IV describe the whole process and include recommendations for further implementations in high-voltage models.

II. Magnetic Design

There are several considerations that must be addressed in designing permanent magnet fault-current limiters (PMFCLs) in order to achieve the current limiting objective, while still featuring "transparency" during nominal grid operation. This objective implies having sufficient impedance during a fault event while exhibiting low impedance for a nominal grid behavior. The change in impedance per phase depends directly on the inductance of the ac coils for that specific phase. Since the inductance depends on the coil's characterizing parameters, essentially $L = \mu N^2 \cdot \frac{A}{l}$ (long solenoid approximation), the relation of the cross section to length as well as the number of windings is a defining factor in the limiting capabilities of the design. The permeability μ, the factor in the heart of the device, can be manipulated by the permanent magnets' saturating fields, responsible for the differing value of impedance between nominal and fault states.

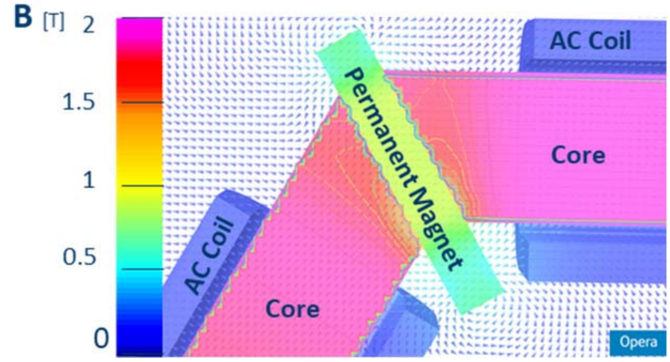

Fig. 1. Map of the magnetic field as simulated in Opera FEA showing the magnet to core interface and the resulting saturating magnetic fields. AC current is not present in the figure shown.

The cross-sectional ratio of the permanent magnets to magnetic core areas is also of defining importance, responsible for the level of saturation achieved in the core due to the magnetic fields induced by the permanent magnets. While this is an important factor to design for in all saturated core FCLs [5], [18], when implementing permanent magnets, this factor becomes crucial. If the calculations are not exact for the inductive requirements in a conventional saturated FCL (SFCL), adjustments can be made in the biasing currents in the dc coils. Because this cannot be done when using permanent magnets as a means for biasing, this requires unerring calculations for the required ratios to be used for the design.

In order to achieve deep saturation within the cores [for grain-oriented electrical steel (GOES) this occurs at a value of $\approx 2T$] from high-grade permanent magnets with remanence fields of $\sim 1.4\ T$ (e.g., NdFeB grade N52), the magnet to core cross-section ratio should approach a ratio of 2:1. This concentrates the magnetic field vectors, increasing their density within the iron core. Fig. 1 shows the magnetic field as simulated in Opera finite-element analysis (FEA) showing the cross-section magnet to core ratio. The figure shows the cross-sectional effects on the saturating field. The line map contours show the equal levels of magnetic field values. As the distance from the permanent magnet increases, the density of the vector field also increases, thus achieving a full saturation of 2 T by the point of reaching the core section under the coils.

Apart from the optimization of permanent magnets to create an effective PMFCL device, it is a challenge to design PMFCL devices implicitly to be capable of limiting symmetrical, three-phase faults. It is the common idea to extend the capabilities for three phases by utilizing three separate single-phase devices [19]. While this is, of course, feasible, this inherently does not produce a design of maximum efficiency, measured by the volume of materials needed to current-limiting capability. Several three-phase designs have been proposed [20], [21], however, to take into account the design for the advantages and disadvantages of permanent magnets, an alternative novel approach incorporating the above-presented factors is shown in Fig. 2. Each adjoining core couple shown in Fig. 2 is responsible for a single phase, resulting in circular symmetry.

The magnetic field orientation displayed in Fig. 2 reveals the implementation of a unidirectional dc magnetic-flux path.

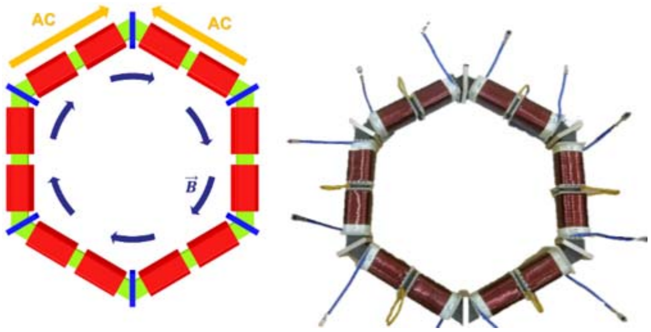

Fig. 2. Prototype design of permanent magnet FCL (PMFCL) capable of limiting three-phase faults. Green shows the GOES core, blue indicates the permanent magnets with their orientation tangent to the radius. Every two adjacent sections are connected in series with a single phase. Yellow arrows show the connected orientation of the ac coils. Dark blue arrows show the closed magnetic loop (during nominal performance).

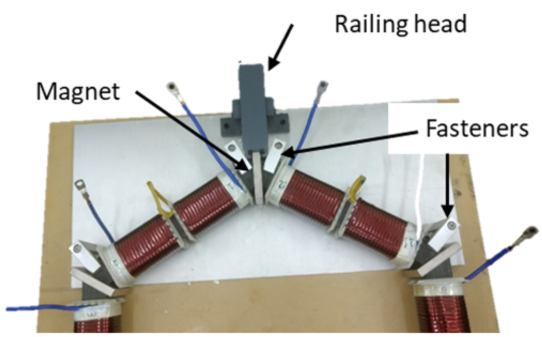

Fig. 3. Assembly of the PMFCL device.

This is done by causing the magnetic field to travel continuously through the whole device, eliminating any magnetic "flip zones" where the field must create a 180° rotation. Not having to incorporate these zones allows for a more compact design [22]. However, the assembly process is presumed more challenging due to the strong uniform magnetic forces, without any opposing magnetic fields mitigating the forces between the magnets and cores. Yet, because of this model's symmetry, the assembly process is simplified. Since the permanent magnets are all placed with the same orientation, with a 60° angle to close the loop, each position of the magnets is also the most energetically desired position for the magnet to be, i.e., centered between two core pieces where the magnetic field is aligned. This is analogous to the case when two separate permanent magnets snap together they do so in a symmetric way always aligning their magnetic centering forces. This led to a relatively simple assembly process illustrated in Fig. 3, where the only need was to create a railing to direct the magnets to their position without introducing undesired angles with no additional restraining forces involved. Fasteners hold the GOES core in place, while a railing head directs the entry position of the permanent magnet. Once the magnet begins to "feel" a substantial attraction force, it "jumps" into a place at the exact desired position. The side of the device that was assembled is rotated to fasten the adjoining cores and the process is repeated for the other sides.

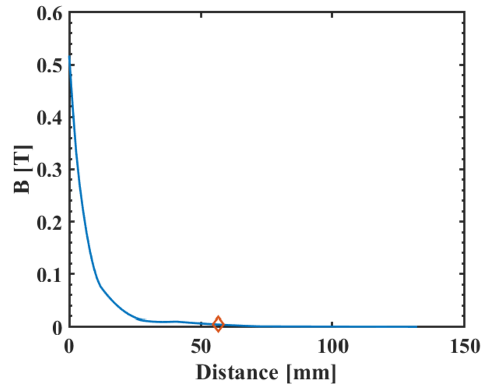

Fig. 4. Simulated measurement of the stray field from the PMFCL device. The strongest stray fields are from the magnets in the demagnetization direction. The measurement was simulated using Opera FEA and confirmed with a probe measurement. Diamond shows the 5-Gauss point.

Once the whole setup is in place, a slight force is applied to move the permanent magnets toward the center of the structure. This was shown to lower the nominal losses by increasing the saturation of the cores at crucial points along the ac coils. The friction between the permanent magnets and the cores was enough to keep the decentering in place.

Once the PMFCL three-phase device is completed, the stray field is almost negligible, reaching the safety limit of 5 Gauss at a distance of 5.5 cm from the magnets. Fig. 4 presents data of the stray field as a function of the distance from a permanent magnet situated in the PMFCL calculated by magnetic simulations. The diamond marker shows the 5-Gauss point. The simulated data were verified with the measurement of the magnetic field as a function of the distance from the permanent magnet situated in the PMFCL.

III. Results of Measurements

As the main function of this device is to induce variable impedance depending on the current value, it is important to characterize experimentally the impedance as a function of the current [2], [23]. This is done by producing a ramp-up current in a single phase and calculating the inductance from the measured differential voltage [24]

$$V_{FCL} = \frac{d}{dt}(LI). \tag{1}$$

By integrating on both sides

$$L_{(t)} = \frac{\int V_{PMFCL} dt}{I}. \tag{2}$$

The results for this measurement, across two ac coils for a single phase, are presented in Fig. 5 where the inductance is shown as a function of current in the ac coils.

The curve demonstrates a high inductance experienced in the range of 20–160 A. The range below 20 A defines the nominal current domain, where virtually no current limiting is taking place. Past 160 A, the inductance begins decreasing due to the magnetization of the core in the opposing direction due to the high opposing current in the ac coils, reducing also the voltage drop across the device. This limit presents the

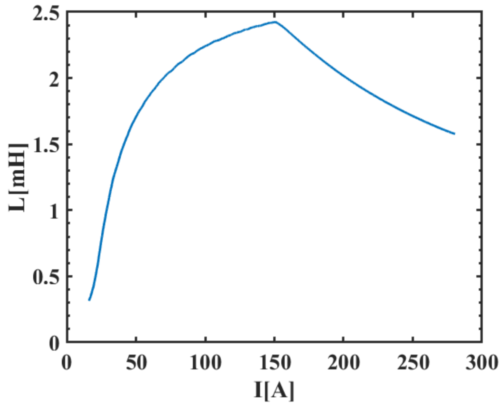

Fig. 5. Inductance measurement of two ac coils for a single phase within the three-phase device. Measurement was done by inducing a rising current ramp and calculating the inductance.

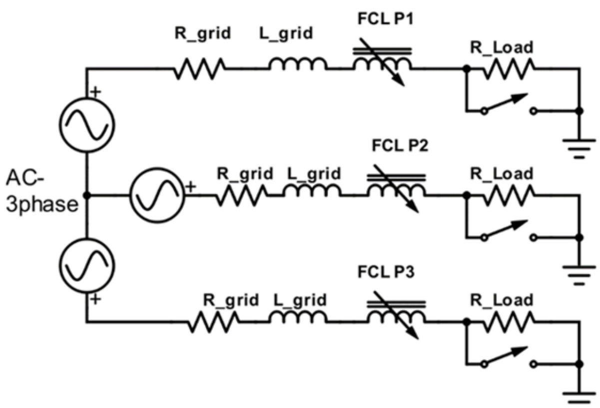

Fig. 6. Nominal grid measurement schematics and values of the various components are given in Table I.

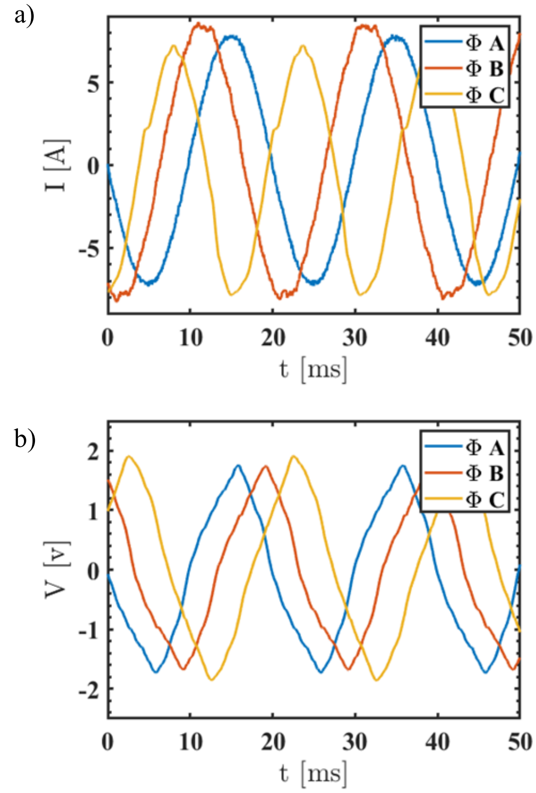

Fig. 7. Nominal measurement results for the triple-phase PMFCL device. (a) Current values on each phase. (b) Voltage values on each phase.

maximum current-limiting capability of our laboratory-scale device. Full reverse saturation will result in inductance equal to initial values with no current. Below 20 A, the points are not plotted due to the challenge in measuring these points in a transient state of the device. To produce accurate results for these points, the inductance should be measured for constant nominal current values.

While this method provides the data to determine the device performance and capabilities, real-time nominal and fault measurements are also important to prove the concept. The following measurements present these results and a comparative analysis of the phase-coupling effects in the three-phase device. It is important to note that the inductance measurement of a single phase is accurate under the assumption that the phase-coupling effects are negligible. A full analysis of the method for the inductance measurement is explained in [24].

The measurements done to provide the behavior of the device during the nominal state include two variations. First, the full three-phase nominal measurement, where the nominal current flows through all three phases. Second, with a single-connected nominal phase with a simple probe measurement on the adjacent ac coils to measure the phase-coupling effects during nominal grid performance.

The three-phase nominal measurement was performed on an experimental model grid as shown in Fig. 6. Each phase segment on the PMFCL was connected in series with a separate load per phase. The grid resistance and inductance are illustrated in the schematics in series with each phase of the PMFCL accordingly. After each phase, the current travels through a resistive load and back through the neutral/ground. Results, shown in Fig. 7, present the voltage and current waveforms measured across all three phases with an average rms current of 5.4 A and voltage of 1.1 V producing a voltage drop of 0.5% from the total grid voltage. This result illustrates the practical transparency of the PMFCL to the grid under nominal conditions as it consumes very little reactive power and practically negligible active power. The slight deviations from a sine waveform are inconsequential in relation to the waveform of the tested grid, signal analysis measured total harmonic distortion (THD) of 0.08%.

The second nominal measurement was done by connecting a single phase to the grid while conducting measurements on an adjacent phase disconnected from the circuit. This measurement produced the results shown in Fig. 8, amounting to a 0.25% voltage drop across the adjacent phase. During nominal grid behavior, this amount is negligible, however, as indicated by fault measurements; when the currents reach high levels, this causes distinct-coupling effects.

The ultimate test of success for the triple-phase PMFCL is determined by the fault limiting capabilities during a fault grid state. These measurements were done on the modeled

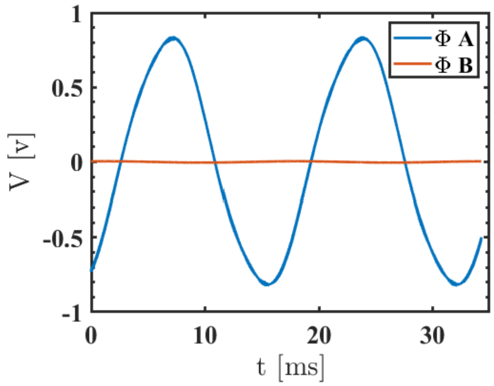

Fig. 8. Phase coupling during nominal state measurement. ΦA is the nominal phase measured in volts and ΦB is the adjacent disconnected phase measured in millivolts.

TABLE I
PARAMETERS OF LABORATORY MODELED THREE-PHASE GRID

Parameter	**Value**
Voltage rms [v]	230
Frequency [Hz]	50
Grid inductance, $\boldsymbol{L_{grid}}$[mH]	2.29
Grid resistivity, $\boldsymbol{R_{grid}}$ [$\boldsymbol{\Omega}$]	0.78
Normal grid load, $\boldsymbol{R_{Load}}$ [$\boldsymbol{\Omega}$]	41

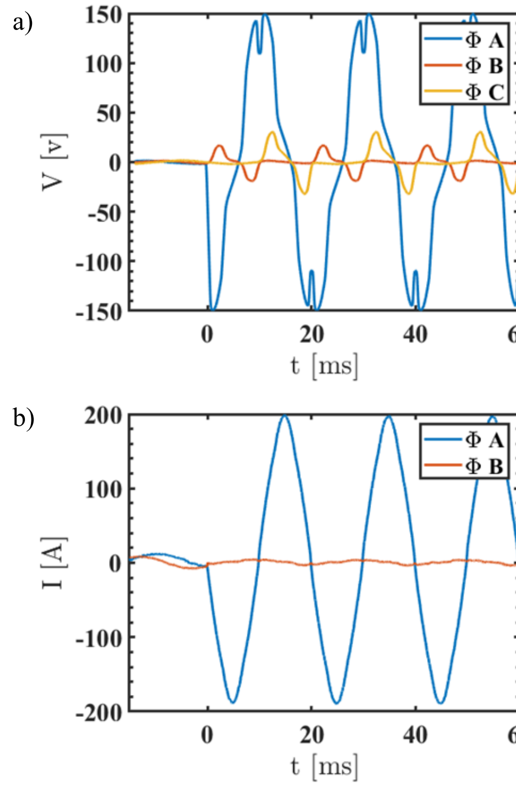

Fig. 9. Measured data for single-phase fault on the triple-phase PMFCL device. (a) Voltage measurements. (b) Current measurements.

grid described in Fig. 6, with the use of short-circuit switches and the resistive loads for each phase separately. The values of the various components in the figure are given in Table I. Several fault state variations were tested to replicate fault states in individual phases and to show how the device reacts as a whole, for each individual case.

Measurements were done by first connecting all phases with a nominal load resistance and introducing a fault current by closing the switches shown in Fig. 6, thus shorting the load to the neutral. Fig. 9 presents the fault measurement across phase ΦA with phases ΦB and ΦC kept with their load in their nominal state.

It is worth noting the zero delay in limiting the fault current. As ΦA enters the fault mode, the specific core length exits its saturation, resulting in a simultaneous voltage increase on the ac coil. The actual delay is a derivative of the flipping magnetic domains within the core material, several orders of magnitude faster than the voltage response. This is shown in Fig. 9(a) as the first minimum peak for ΦA. It is also apparent that the signature voltage dip when crossing zero current experienced during the fault state in FCLs [7]. The results prove exceptionally well, achieving a limiting current of 132 A [Fig. 9(b)], which is less than 30% of the prospected fault current (440 if no limiting was present during the fault). The voltage across the fault phase was measured with a 45% voltage drop of the total phase voltage (99.3 V of 220 V). Also evident is the small coupling with the adjacent phase. The current in this adjacent phase, which performs under nominal conditions, increases to 6.4 A rather than the nominal 5.3 A [Fig. 9(b)]. While this is a notable increase, it is still within the nominal current levels.

The single-phase fault was tested individually for each phase on the device, showing identical limiting results for each phase. This type of fault, asymmetrical single-phase-to-earth, is also noted as the most common type, amounting to 70%–80% of all faults [25].

Next, the double-phase fault was tested, shorting the resistive loads on phases ΦA and ΦB simultaneously. The results are shown in Fig. 10. Note that the asymmetry of the voltage waveforms as a result of the strong phase coupling experienced with a phase delay between adjacent phases. From Fig. 10(a), it is clear that the phase coupling not only effects the nominal phase strongly but also has an effect on the second fault phase, causing the characteristic dip in voltage as being the long-range. High γmf value from the fault phase is powerful enough to slightly desaturate the adjacent phase's core, causing the rise in inductance on the unfaulted phase.

We measured a nominal current in the adjacent phase with THD of 0.4% to a perfect sine wave, shown in Fig. 10(b), which is satisfactory for most power needs. The values recorded for the fault phases were 128 A limited current, 29% of the prospected fault current, with 45% voltage drop on each phase from the grid voltage per phase. Nominal phase ΦC recorded 5.14 A current, with 10% voltage drop across the phase ac coils. Fig. 11 provides some intuition to the phase-coupling effects due to the saturating fields of adjacent magnetic cores. In the pictured state, two phases (top right) are simultaneously in a reversed saturation while their adjacent cores (clockwise and anticlockwise to them) reveal a slight desaturation of the cores near the magnets.

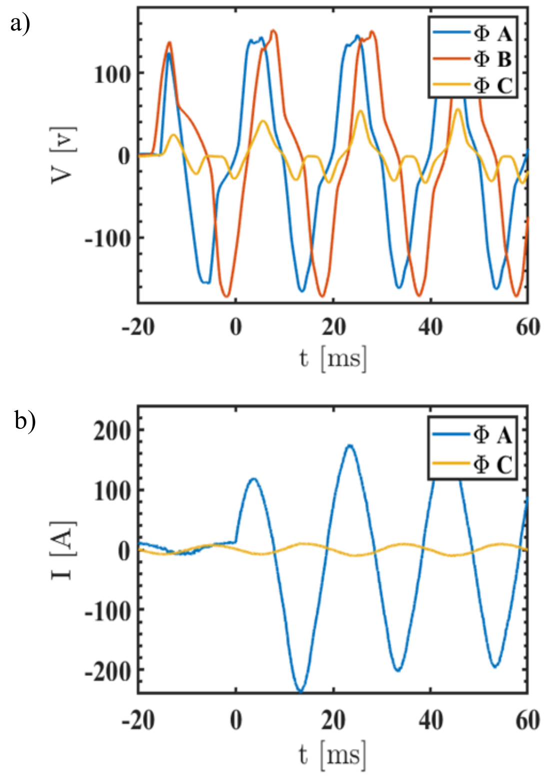

Fig. 10. Measured data for double-phase fault on the triple-phase PMFCL device. (a) Voltage measurements. (b) Current measurements.

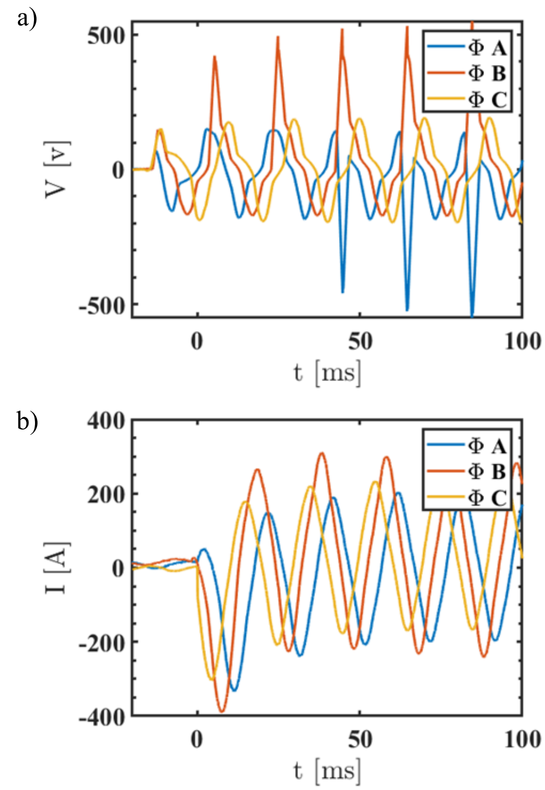

Fig. 12. Measured data for triple-phase fault on the triple-phase PMFCL device. (a) Voltage measurements. (b) Current measurements.

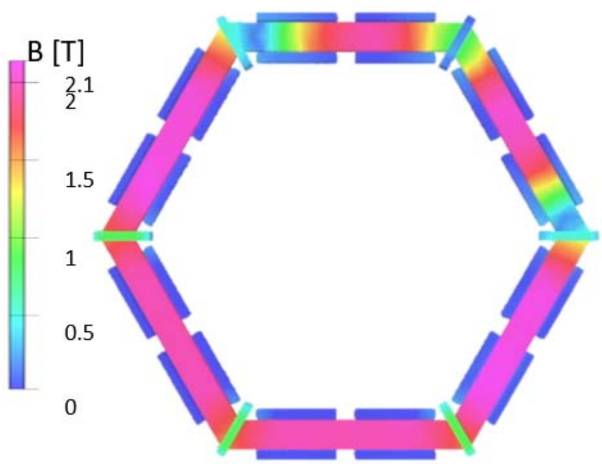

Fig. 11. Magnetic-field map during a double-phase fault simulation.

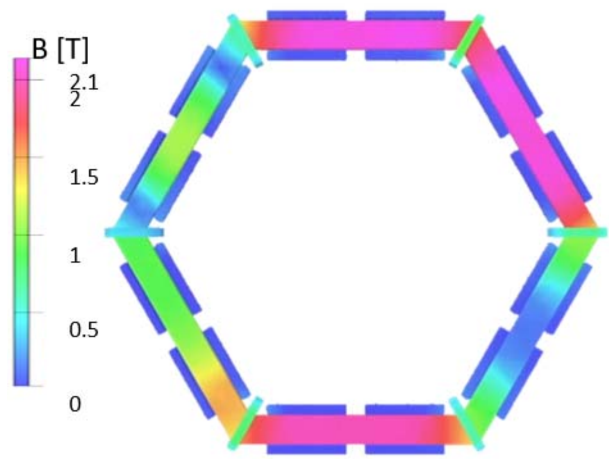

Fig. 13. Magnetic-field map during a triple-phase fault simulation.

The final measurement is the case of a three-phase fault. For this step, all three loads are shorted simultaneously, resulting in a symmetrical three-phase-to-earth fault. This type of fault occurrence is recorded in 2%–5% of the total system faults [25] and as cited, however rare, if this fault occurs, it is responsible for the most cause of damage. Given the unique simplicity of the device, with zero-switching components and compactness, we were able to create this type of symmetrical fault simultaneously with relative ease. It is noted [25] that most symmetrical faults are merely analyzed per phase by simply calculating the potential effects with Thevenin's theorem, which is due to the complexity of most fault current limiting systems combined with creating a symmetrical three-phase fault.

It is easy to identify the initial symmetry of the fault event by the initial peak in the voltage measured for each phase [see Fig. 12(a)]. After noticing the initial symmetry of the fault voltage, the remaining waveform behaves unusual, varying drastically from the previous fault tests. The interesting part with the PMFCLs is that during a fault event, the permanent magnets have no inherited application in saturating the cores, rather their task is to limit the phase-coupling effects. This is presented visually in the simulation of the magnetic-field map in Fig. 13 where the magnets provide isolation of the desaturating magnetic fields in the fault phases. This assures that a single fault does not eventually develop into a multi-phase fault. This means that with all of the aberrations considered, the current graph in Fig. 12(b) still presents a 30%–40% limited current of the prospected fault current. Other than this, the current values measure an $r^2 \approx 92\%$ deviating from a perfect sine function. The recurring spikes shown in Fig. 12 are likely due to the mechanical vibrations of part of the magnetic core limbs due to the strong magnetic forces experienced and insufficient mechanical reinforcement of this test model. After testing several symmetrical triple phase fault events, the PMFCL device deformed slightly due to the forces involved. Future designs should take into consideration the reinforcement of the device to withstand the fault-current forces.

IV. Summary and Conclusion

A triple-phase PMFCL device was simulated, built, and tested. The results achieved have shown the capabilities of this type of design (patent pending [26]), promoting the importance of applying each consecutive phase to help strengthen the overall limiting effects, and its overall potential for implementation in future devices. A full three-phase fault test was done, showing the behavior of such an event without relying on analytical predictions. Triple-phase simulations with FEA proven accurate in predicting the capabilities of the device. However, simulations did not account for the force vibrations that occur during fault events, as well as the strong phase coupling experienced. More attention should focus on minimizing the coupling effects in such three-phase devices. An important advantage to the design described here is due to the uniform magnetic orientations, the assembly process is relatively simple, allowing for scaling up of the proposed design for high power grids while still maintaining relative compactness by optimizing the magnetic paths. We thus conclude by recommending that future devices will consider the fundamental aspects described here, such as the permanent magnet to core ratio, unidirectional magnetic paths, and variable coil winding densities.

Acknowledgment

This work was supported in part by the Israeli Ministry of National Infrastructure, Energy and Water Resource under Grant 214-11-004.

References

[1] A. Naamane and N. K. Msirdi, “Towards a smart grid communication,” *Energy Proc.*, vol. 83, pp. 428–433, Dec. 2015.

[2] A. Abramovitz, K. M. Smedley, F. D. L. Rosa, and F. Moriconi, “Prototyping and testing of a 15 kV/1.2 kA saturable core HTS fault current limiter,” *IEEE Trans. Power Del.*, vol. 28, no. 3, pp. 1271–1279, Jul. 2013.

[3] L. Wei *et al.*, “Performance investigation and optimization of a novel hybrid saturated-core fault-current limiter considering the leakage effect,” *Energies*, vol. 11, no. 1, p. 61, Jan. 2018.

[4] P. A. Commins and J. W. Moscrop, “Analytical nonlinear reluctance model of a single-phase saturated core fault current limiter,” *IEEE Trans. Power Del.*, vol. 28, no. 1, pp. 450–457, Jan. 2013.

[5] J. W. Moscrop, “Experimental analysis of the magnetic flux characteristics of saturated core fault current limiters,” *IEEE Trans. Magn.*, vol. 49, no. 2, pp. 874–882, Feb. 2013.

[6] B. Chen, L. Wei, C. Tian, Y. Lei, and J. Yuan, “Parameter design and performance investigation of a novel bridge-type saturated core fault current limiter,” *IEEE Trans. Power Del.*, vol. 32, no. 2, pp. 1049–1057, Apr. 2017.

[7] Y. Nikulshin, Y. Wolfus, A. Friedman, and Y. Yeshurun, “Dynamic inductance in saturated cores fault current limiters,” *J. Supercond. Novel Magn.*, vol. 28, no. 2, pp. 579–583, 2015.

[8] *GridOn*. [Online]. Available: Accessed: Jun. 1, 2018. http://www.gridon.com/index.html

[9] Y. Nikulshin *et al.*, “Saturated core fault current limiters in a live grid,” *IEEE Trans. Appl. Supercond.*, vol. 26, no. 3, 2016, Art. no. 5601504.

[10] S. C. Mukhopadhyay, F. P. Dawson, M. Iwahara, and S. Yamada, “Analysis, design and experimental results for a passive current limiting device,” *Proc. Inst. Elect. Eng.-Electr. Power Appl.*, vol. 146, no. 3, pp. 309–316, May 1999.

[11] A. Ramadan, “Permanent magnet fault current limiter for the power grid,” *Proc. Energy*, vol. 134, pp. 768–775, Oct. 2017.

[12] J. Hall and A. Cheer, “Full-scale 11kV fault current limiter for the distribution grid based upon zero power consumption ceramic ferrite permanent magnets,” *CIRED*, vol. 23, pp. 15–18, Jun. 2015.

[13] L. Wei *et al.*, “Performance and optimization study of a novel compact permanent-magnet-biased fault current limiter,” *IEEE Trans. Magn.*, vol. 53, no. 11, Nov. 2017, Art. no. 8401404.

[14] J. Yuan *et al.*, “Performance investigation of a novel permanent magnet-biased fault-current limiter,” *IEEE Trans. Magn.*, vol. 51, no. 11, Nov. 2015, Art. no. 8403004.

[15] B. Chen *et al.*, “Investigation on a modified hybrid compact saturated-core fault current limiter based on permanent magnets,” in *Proc. IEEE Conf. Electromagn. Field Comput. (CEFC)*, Nov. 2016, vol. 49, no. 7, p. 1.

[16] J. Yuan, Y. Lei, L. Wei, C. Tian, B. Chen, and Z. Du, “A novel bridge-type hybrid saturated-core fault current limiter based on permanent magnets,” *IEEE Trans. Magn.*, vol. 51, no. 11, Nov. 2015, Art. no. 8401904.

[17] Z. Liang, L. Qing-Min, L. Hong-Shun, and W. H. Siew, “Study on the feasibility of developing high voltage and large capacity permanent-magnet-biased fault current limiter,” in *Proc. 44th Int. Univ. Power Eng. Conf. (UPEC)*, Sep. 2009, pp. 1–5.

[18] N. Vilhena, P. Arsénio, J. Murta-Pina, A. Pronto, and A. Álvarez, “A methodology for modeling and simulation of saturated cores fault current limiters,” *IEEE Trans. Appl. Supercond.*, vol. 25, no. 3, Jun. 2015, Art. no. 5600704.

[19] S. C. Mukhopadhyay, F. P. Dawson, M. Iwahara, and S. Yamada, “A novel compact magnetic current limiter for three phase applications,” *IEEE Trans. Magn.*, vol. 36, no. 5, pp. 3568–3570, Sep. 2000.

[20] M. Eladawy and I. A. Metwally, “A novel five-leg design for performance improvement of three-phase presaturated core fault-current limiter,” *IEEE Trans. Magn.*, vol. 54, no. 7, Jul. 2018, Art. no. 8001410.

[21] M. Arab Baferani, M. R. Chalaki, N. Fahimi, A. A. Shayegani, and K. Niayesh, “A novel arrangement for improving three phase saturated-core fault current limiter (SCFCL),” in *Proc. IEEE Texas Power Energy Conf. (TPEC)*, Feb. 2018, pp. 1–6.

[22] B. C. L. Wei, C. Tian, Y. Gao, K. Muramatsu, and J. Yuan, “Optimization study of a novel small-section permanent-magnet-biased fault current limiter with leakage flux effect,” in *Proc. IEEE Conf. Electromagn. Field Comput. (CEFC)*, vol. 3, Nov. 2016, p. 1.

[23] Y. Nikulshin, Y. Wolfus, A. Friedman, and Y. Yeshurun, “Improving the performance of saturated cores fault current limiters by varying winding density in the AC coils,” *IEEE Trans. Appl. Supercond.*, vol. 25, no. 3, Jun. 2015, Art. no. 5602705.

[24] J. Linden, Y. Nikulshin, A. Friedman, Y. Yeshurun, and S. Wolfus, “Design optimization of a permanent-magnet saturated-core fault-current limiter,” *Energies*, vol. 12, no. 10, p. 1823, May 2019.

[25] (Nov. 12, 2015). *Types of Faults in Electrical Power Systems*, pp. 1–5. [Online]. Available: https://www.electronicshub.org/types-of-faults-in-electrical-power-systems/

[26] S. Wolfus, J. Linden, Y. Nikulshin, and Y. Yeshurun, “Fault current limiter with saturated core and permanent magnet,” U.S. Patent 62 683 752, 2018.